GENERAL PHYSICS

I. MOLECULAR BEAMS*

Academic and Research Staff

Prof. J. R. Zacharias	Dr. J. R. Clow	Dr. R. C. Pandorf
Prof. J. G. King	Dr. D. S. Hyman	F. J. O'Brien

Graduate Students

T. R. Brown	G. A. Herzlinger	D. S. Ofsevit
S. A. Cohen	M. R. Koolish	T. A. Postol
W. B. Davis	J. W. McWane	R. F. Tinker
	D. E. Oates	

A. OBSERVATION OF THE VORTEX STATE IN NIOBIUM BY MEANS OF AN ATOMIC BEAM

1. Introduction

Magnetic field variations near the surface of a superconducting Nb cylinder in a transverse magnetic field have been observed by passing a state-selected beam of Potassium atoms over the surface of the cylinder. Figure I-1 is a schematic diagram of the apparatus. The beam is chopped by a rotating, 4-slotted wheel, and the arrival time of an atom at the hot Platinum wire detector is measured by an ND 180M multichannel analyzer (MCA) operating in the multiscaling mode and triggered by a signal at a fixed time (0.85 ms) after the chopper is open. An electron multiplier and pulse amplifier enable us to count single atoms.

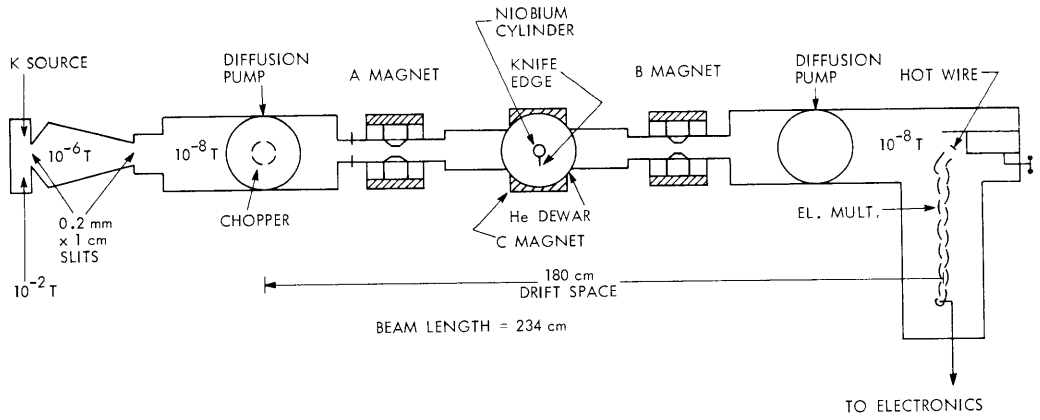

Fig. I-1. Apparatus for studying variations in superconductor's surface field.

*This work was supported by the Joint Services Electronics Programs (U.S. Army, U.S. Navy, and U.S. Air Force) under Contract DA 28-043-AMC-02536(E), and in part by the Sloan Fund for Basic Research (M.I.T. Grant 249).

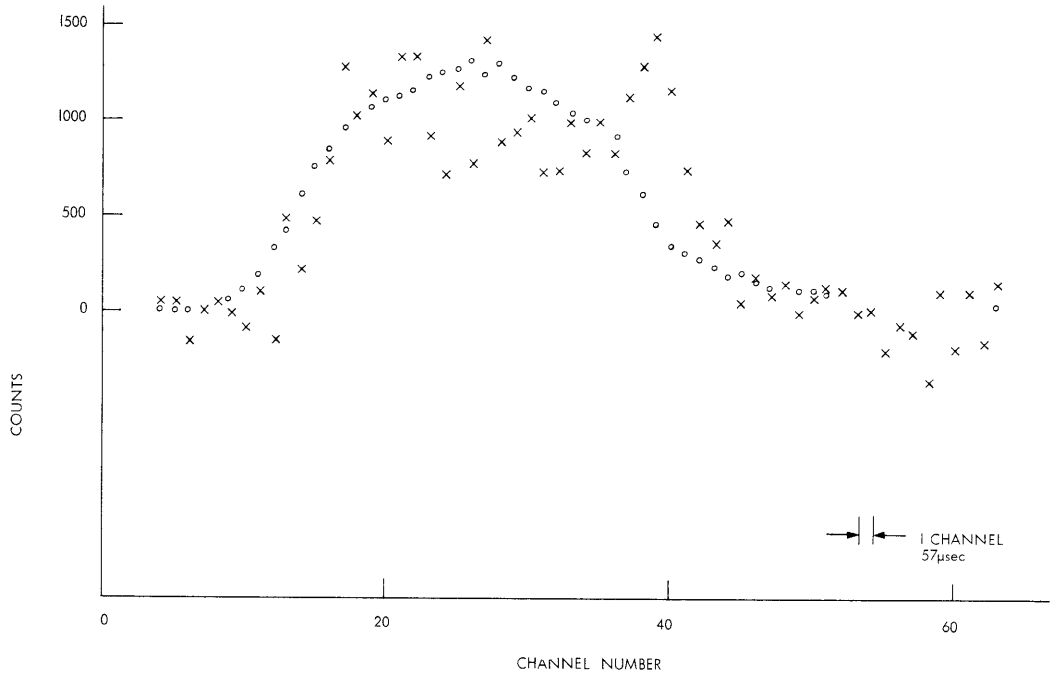

Fig. I-2. Result (indicated by crosses) of subtracting an MCA scan of 85 min at H = 3200 Oe from one at H = 2075 Oe.

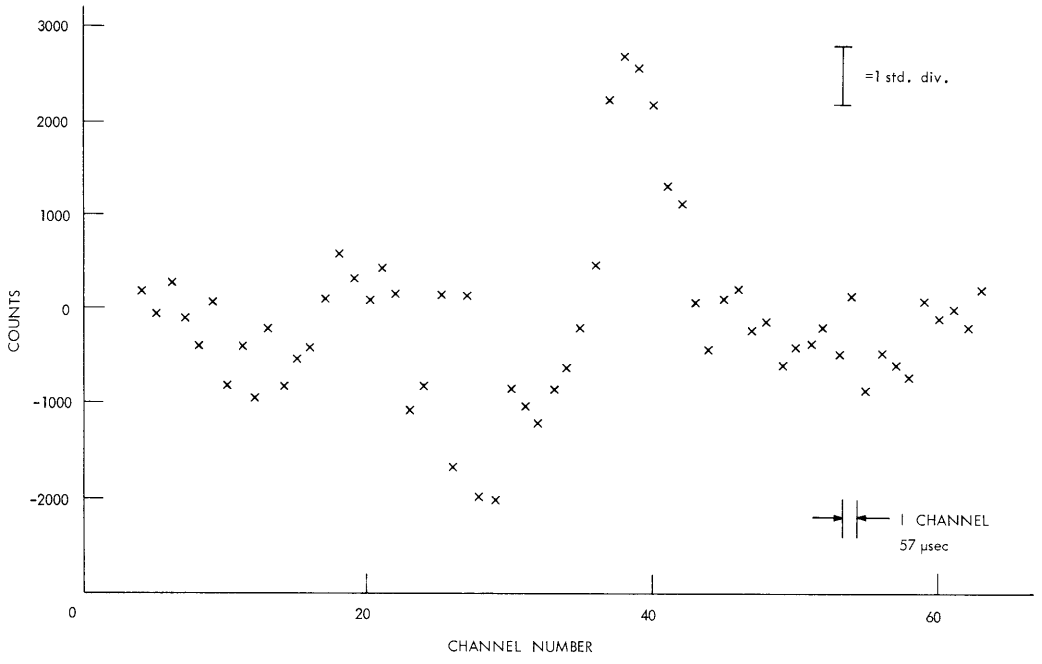

Fig. I-3. Sum of difference between crosses and dots in Fig. I-2 for 4 different curves.

The atoms passing near the Nb cylinder see a time-variant field with Fourier components at frequency v/l, where v is the velocity, and l the wavelength of a spatial variation in the field. Thus one would expect to see peaks in the velocity distribution of the flopped atoms corresponding to those periodicities present in the magnetic field of Nb.

2. Discussion

The crosses in Fig. I-2 are the result of subtracting an MCA scan of 85 min at H = 3200 Oe from one at H = 2075 Oe. At the temperature of the sample (4.3 °K) the critical field is ~2600 Oe, so at 3200 Oe there should be no lattice. When corrected for the diamagnetism of the cylindrical sample H = 2075 Oe corresponds to B = 1750 G. In order to have a better chance of getting a good lattice, the magnetic field was turned on while the sample was still at 77 °K and left on as Helium was transferred into the dewar.

Because of a change in oven pressure between the scans the velocity-dependent background was slightly larger in the H = 2075 Oe scan. The size of this residual background is determined by integrating both scans to find the change in intensity. An appropriately normalized background curve is subtracted from the data. These are the dots in Fig. I-2. They represent the H = 3200 Oe curve multiplied by 0.111. The normalizing factor is slightly too large because the signal is included in the integration, thereby making the total intensity appear larger for the H = 2075 Oe scan. When this effect is taken into account the dots appear to be an even better fit to the crosses over the curve except for the narrow peak. This correction has not been completed for all four of the chopper openings but should be soon.

Figure I-3 is the sum of the difference between the crosses and the dots in Fig. I-2 for four different curves, all of them similar to Fig. I-2. These correspond to the four different slots in the beam chopper. It is necessary to keep these distinct because their positions on the chopper wheel are not quite symmetrical, which causes a slight shift in apparent arrival time. This effect is significant in the initial subtraction, but not in the later additions. There is a small residual background peak left in Fig. I-3 caused by the presence of the signal. The narrowness of the peak makes it almost certain that it is produced by the lattice, rather than being some spurious effect such as Majoran flop, bouncing off a wall, and so forth. Any other possible cause of increased signal has a fairly wide velocity dependence and would be expected to increase the counting rate over a much larger spread in arrival times.

The peak is approximately the right width and size, and is within the spread in arrival times expected for this magnetic field. This uncertainty in arrival time comes from two sources. One is the possible variation of angular orientation of the lattice relative to the beam velocity. This may be fixed by pinning sites or it may vary from run to run, but in any case it is not known. (Another possibility is many patches of lattice at different orientations. If a uniform angular distribution is assumed, then most of the signal

(70%) is at an arrival time corresponding to a fixed orientation, where the velocity vector is parallel to a vector from one lattice point to the next.) The other uncertainty is connected with the theoretical problem of a K atom going through such a complex field. An expansion for the field in terms of reciprocal lattice vectors has been worked out but, thus far, we have only been able to guess that the smallest K, $4\pi d/\sqrt{3}$, where d is the lattice spacing, is dominant in flopping atoms because its component extends farther from the surface of the sample than any other reciprocal lattice vector.

$K = 4\pi/\sqrt{3}\, d$ would correspond to a peak at channel 51, and it is clear that the peak is somewhere around channel 38 or 39. This is much closer to a peak that would be caused by $K = 2\pi/d$ at channel 42. This problem is now being studied by taking a large number of different scans at a single value of the magnetic field to see if the peak remains in the same place or shifts between certain limits.

3. Future Plans

The major difficulty in observing the effect is attributable to the velocity-dependent background, caused apparently by beam-beam scattering, which until recently was so large and variable as to mask the signal. This background was finally reduced by placing the collimating knife edge directly on the surface of the Nb cylinder and allowing surface irregularities to let atoms through. The average slit width is estimated, from the beam intensity, to be ~5000 Å. This still allows approximately five times as much velocity-dependent background through as signal. In the long run a velocity-selected beam will be used which will improve the signal-to-noise ratio. At the moment the necessary electronics to have the MCA punch paper tape is being built. At the same time a program to analyze data on a PDP-1 computer is being written. It should then be possible to take and analyze data at a much faster rate than at the present time. This should enable us to take sufficient data in a reasonable length of time to settle some of the questions raised in this report.

We are also investigating the possibility of applying this technique to the study of other systems in which electric and magnetic fields vary over distances of 100 to 10,000 Å.

T. R. Brown, J. G. King

B. LOW SPHERICAL ABERRATION ELECTRON LENS

The goal of this study of electrostatic lenses for emission electron microscopy, by using computer simulation techniques, was to find a lens capable of resolving individual atoms (separated by distances of the order of 5 Å), with a magnification of approximately 100 serving as the first stage in a system of lenses.

The current state of electrostatic lens design has been limited by the inability to correct the spherical aberration in known lenses. The design innovation explored in this project is the use of a thin diaphragm as an electrode. Present technology is capable of providing thin-film electrodes less than 100 Å thick, and hence this innovation is possible. As a first approximation, problems such as diffraction and scattering that arise with the use of such an electrode have been ignored.

There are several reasons for this study.

1. It demonstrates the possibility of improving the best current electrostatic lens designs.

2. It indicates that emission electron microscopy using "Auger electrons" is possible; particularly, it indicates that enough intensity may be obtainable.

3. Such an electron microscope may be of use, in particular, in the "molecular microscope" that is being investigated by our group.

1. Definitions and Assumptions

As is customary in other publications,[1-3] all lens diagrams in this report show the cross sections of lenses with axial (cylindrical) symmetry. The r and z coordinates are as shown, with the third dimension provided by rotation around the z axis, the axis of symmetry. Note that in the two-dimensional representation, r has both positive and negative values.

2. Object Plane

The "object" to be magnified lies in or near the plane z = 0, the "object plane." This is the cathode of the lens system. The "Auger electrons" which are used to create the image are emitted by the atoms of the object when properly excited.[4] Their approximate "emission energy" E_o depends on the type of atom, as shown in Table I-1. There is a typical spread, ΔE_o, of ±1 eV or less, which must be considered for each value.

Table I-1. Electron emission energies of selected atoms.

Type of Atom	Average Electron Emission Energy E_o (ev)
B	180
C	280
N	390
O	530

3. Focus and Image

The word "focus" has a special meaning in the context of this report. Consider one atom in the object plane that emits several electrons at different angles and/or energies. These electrons pass through the lens with different trajectories. At some point, if the lens is properly designed, these trajectories will approach each other and form an "image" of the atom. At this point of closest approach the trajectories are said to be "focused" (see Fig. I-4).

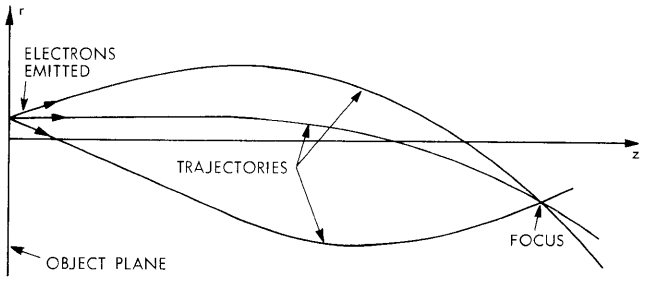

Fig. I-4. Focus.

The electrostatic lens is a set of axially symmetric electrodes, each maintained at a constant voltage. The electrostatic field that is created causes the electron trajectories.

4. Image Plane and Magnification

The "image plane" is that plane where a focus is obtained for an atom located at $(r, z) = (0, 0)$. If the lens is properly designed, the focus for any atom in some desired

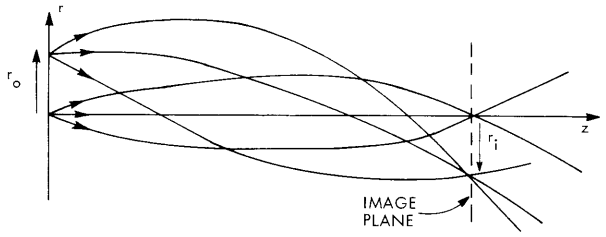

Fig. I-5. Image plane and magnification.

region or the object plane will be close, in some sense, to the image plane (see Fig. I-5). The magnification of the lens is defined as

$$M = \frac{|r_i|}{|r_o|}.$$

In a perfect lens M is independent of r_o. The degree to which M depends on r_o is the distortion of the lens.

5. Resolution and Aberrations

The fact that a set of trajectories will not focus at exactly the same point means that an atom in the object plane will be represented by a spot of some finite size in the image plane. If the spots for two adjacent atoms overlap, the lens will not be useful for work

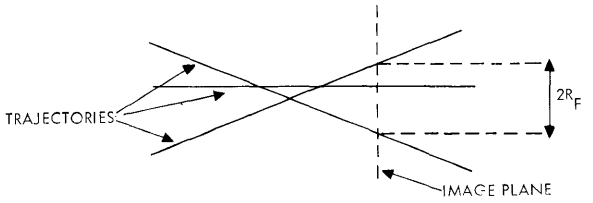

Fig. I-6. Resolution.

on the atomic scale. The measure for the apparent size of an atom in the object plane is the "resolution," as shown in Fig. I-6. R_F is the radius of the spot formed in the image plane. The resolution then is

$$R = \frac{R_F}{M},$$

the apparent size of the object atom. In published works,[5] R_F is the "aberration disc." There are two kinds of aberration: (i) Spherical aberration is caused by different values of the emission angle α_o, which results in R being proportional to α_o^3. (ii) Chromatic aberration is caused by different values of emission energy $E_o \pm \Delta E_o$, which results in R being proportional to $\alpha_o \frac{\Delta E_o}{E_o}$.

The constants of spherical aberration and chromatic aberration will not be discussed. They do not refer to α_o, but to the angle at which the electron enters the lens proper. In the kind of lens discussed here, there is a region between the cathode and the first electrode that is used for acceleration, not for focusing. This region is not part of the lens proper.

6. Calculation of Lens Parameters

The programs used in this project take a given lens design and find the electron trajectories for whatever initial conditions (r_o, z_o, E_o, α_o) the user specifies. It is assumed that the image plane lies in a field-free region, that is, outside the lens. The trajectories in the vicinity of the image plane are then straight lines and can be represented by straight-line equations (see Fig. I-7). The equation for such a line is

$$r = \text{SLOPE}\,(z - \text{CROSS}).$$

Thus for each set of initial conditions (r_o, z_o, E_o, α_o) the programs generate a pair (SLOPE, CROSS).

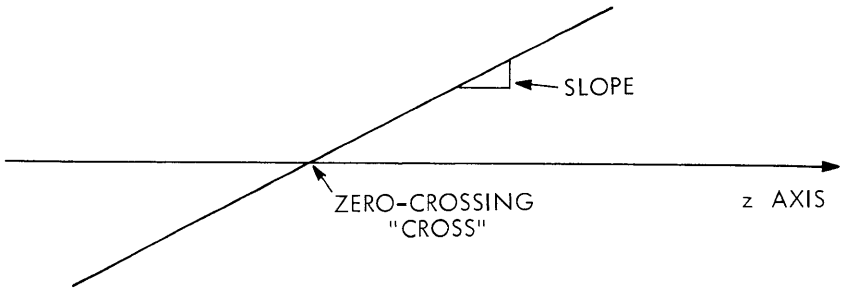

Fig. I-7. Straight-line trajectory parameters.

The lens parameters may then be found: (i) The image plane is located at the value of CROSS for $r_o = 0$ and in the limit $\alpha_o \to 0$. The image plane is different for each E_o. (ii) M can be found for each E_o by setting some r_o with several α_o and noting the average value of r_i (see Fig. I-5). The distortion can be estimated by varying r_o. (iii) R can be calculated by fixing r_o and varying α_o and/or ΔE_o.

7. Study of a Particular Lens Design

The purpose of this project was to evaluate a particular electrostatic lens design and attempt to improve its performance by suggesting changes in the design. The procedure outlined below required much trial and error before it became a systematic routine. In the future the experience gained should make the procedure even more efficient.

8. Particular Lens Design

The lens design examined in this project is shown in Fig. I-8. It is a modification of a design proposed by Seeliger[1]; it differs from Seeliger's design in the addition of electrodes D and E. Seeliger claims a value of $C_s \approx 3$ for his lens; this is one of the lowest values known. Unfortunately, it has $M \approx 3$, and it cannot resolve individual atoms.

It is a commonplace notion that a lens like Seeliger's must be a converging lens. The addition of the thin diaphragm D and electrode E was suggested by Professor E. H. Jacobsen (now in the Department of Biological Sciences, Columbia University). The lens from the diaphragm "on out" acts as a diverging lens which we hope would improve M and R.

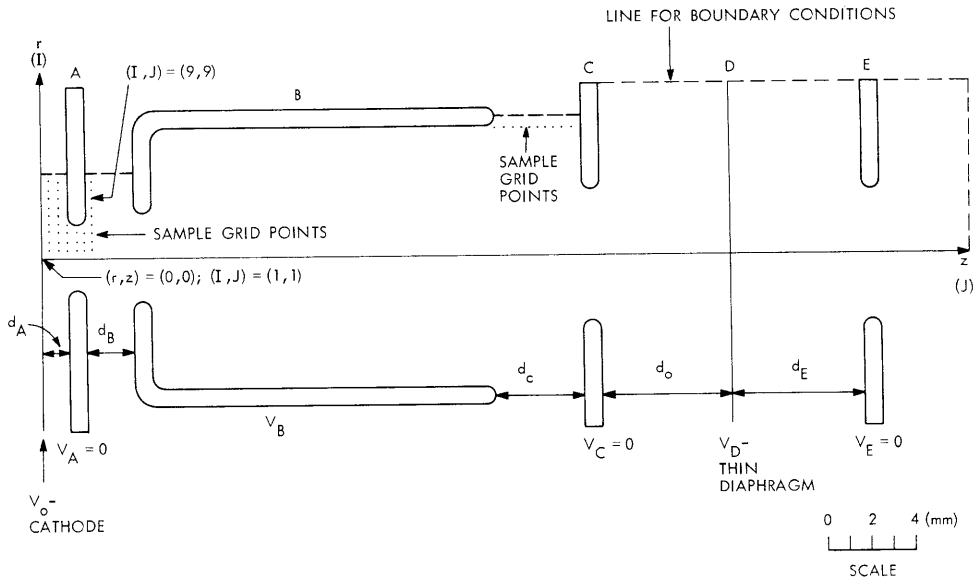

Fig. I-8. Particular lens design analyzed in this project.

9. Design Requirements

The following design requirements were suggested: (i) $M > 50$ ($M > 100$ preferred); (ii) $R \leq 1$ Å (that is, capable of resolving individual atoms); and (iii) $|\nabla\Phi|_{max} \leq$ 150 kV/cm. Requirement (iii) is a limit on the field strength within the lens; 150 kV/cm is the largest value at which the lens could operate continuously. This requirement could be relaxed, but the lens would then have to be operated in a pulsed mode to avoid breakdown. Such a mode would pose additional engineering problems.

The results of this study suggest that requirements (i) and (iii) can be met quite easily. Requirement (ii), however, poses the major problem; this lens does not significantly improve R. We shall suggest several approaches to this problem.

10. Basic Operating Characteristics

Figures I-9, I-10, and I-11 illustrate the basic properties of this lens design. Some initial trial and error was needed to find that $d_A = 1.2$ mm and $V_B/V_o = 0.9$ are satisfactory. $V_o = 18$ kV satisfies requirement (iii). For these runs, d_D and d_E were both set to 6 mm; in the future it will be interesting to find the effect of varying these electrode spacings.

For these figures the initial data were the following.

(i) $r_o = 0$ Å, $z_o = 0$ Å, $E_o = 280$ eV, $\alpha_o = 0.01$ rad; these locate the image plane.

(ii) $r_o = 5$ Å, $\alpha_o = \pm 0.01$ rad, other data unchanged; these enable us to find the magnification.

The fact that SLOPE depends linearly on V_D in (i) (Fig I-9) shows that V_D has a

critical value V_{crit} above which the lens will not focus. CROSS in (i) (Fig. I-10), and M in (ii) (Fig. I-11) both increase quite rapidly as $V_D \rightarrow V_{crit}$ from below. (Note that these are semi-log graphs.) Theoretically, then, M has no limit. Practically, two engineering considerations limit M: (i) High M requires large CROSS; M = 75.2 requires a lens approximately 1.2 m long. (ii) At high M, the stability of V_D becomes critical. The greater M is, the greater $\partial M/\partial V_D$ is (see Fig. I-11).

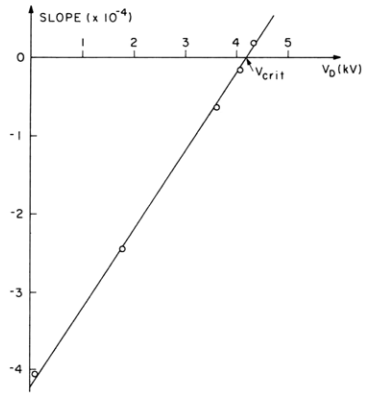

Fig. I-9.
Dependence of SLOPE on V_D.

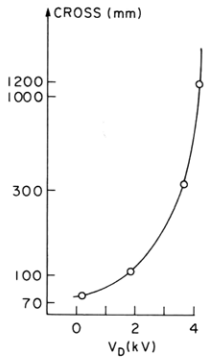

Fig. I-10.
Dependence of CROSS on V_D.

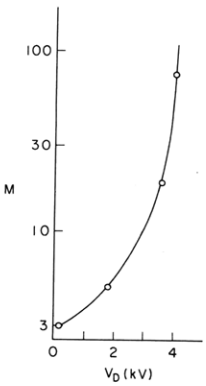

Fig. I-11.
Dependence of M on V_D.

11. Distortion

The distortion of this lens is quite satisfactory, as shown in Table I-2. M varies less than 0.1%, and even this small variance seems to be caused less by the lens than by roundoff errors in the calculation.

Table I-2. Distortion at E_o = 280 eV, α_o = 0.01 rad.

r_o (Å)	M
5	75.2
10	75.1
20	75.2
50	75.2
100	75.2

12. Spherical Aberration

The spherical aberration for this lens shows the expected dependence[3] on α_o for the range of α_o shown in Table I-3. For $\alpha_o \geq 0.01$ rad, R < 1 Å and requirement (ii) is not satisfied.

Table I-3. Resolution for E_o = 280.0 eV, r_o = 0.

α_o (rad)	R (Å)
0.01	2.6
0.02	26
0.04	221
0.06	752

13. Chromatic Aberration

The chromatic aberration of this lens shows the expected linear dependence on ΔE_o, as shown in Table I-4. This aberration is quite considerable and also fails to satisfy requirement (ii).

Table I-4. Resolution for α_o = 0.01 rad, r_o = 0.

E_o (eV)	ΔE_o (eV)	R (Å)
279, 281	1	127
279.5, 280.5	0.5	67

14. Different Types of Atoms

The effect of electrons from other types of atoms on this lens is summarized in Table I-5. It is apparent that when electrons from one type of atom are focused, those from other types of atoms will not be focused in that image plane (if they are focused at all). This is a most useful feature; it is apparent that by "tuning" V_D we can look at one type of atom at a time at a fixed image plane.

Table I-5. Effect of different E_o.

E_o (eV)	Location of Image (mm)	M at Image
180	220	12.9
280	1200	75.2
390	none	no focus
530	none	no focus

D. S. Ofsevit

References

1. P. Grivet, Electron Optics (Pergamon Press, London, 1965), pp. 460-461.
2. A. Illenberger, "Erweitere Möglichkeiten in der Emissions-Elektronenmikroskopie durch Anwendung hoher Feldstärken," Mikroskopie, Vol. 19, No. 11/12, pp. 316-343, 1964.

3. A. Septier (ed.), Focusing of Charged Particles, Vol. 1 (Academic Press, New York, 1967), see particularly, C. Weber, "Numerical Solution of Laplace's and Poisson's Equations and the Calculation of Electron Trajectories and Electron Beams," Sec. 1.2, pp. 45-99.

4. E. H. S. Burhop, The Auger Effect and Other Radiationless Transitions (Cambridge University Press, London, 1952).

5. K.-J. Hanszen and R. Lauer, "Electrostatic Lenses," in A. Septier (ed.), op. cit., Sec. 2.2, pp. 251-307.